RESEARCH ARTICLE | MAY 23 2022

Polarization-pinning in substrate emission multi-mode vertical-cavity surface-emitting lasers using deep trenches

Danqi Lei; Dae-Hyun Kim ; Nasser Babazadeh; David T. D. Childs ; Richard A. Hogg

Appl. Phys. Lett. 120, 211102 (2022)
https://doi.org/10.1063/5.0087166

Applied Physics Letters ARTICLE scitation.org/journal/apl

Polarization-pinning in substrate emission multi-mode vertical-cavity surface-emitting lasers using deep trenches

Cite as: Appl. Phys. Lett. **120**, 211102 (2022); doi: 10.1063/5.0087166
Submitted: 2 February 2022 · Accepted: 14 May 2022 ·
Published Online: 23 May 2022

Danqi Lei,[1] Dae-Hyun Kim,[1,a)] Nasser Babazadeh,[2] David T. D. Childs,[1,3] and Richard A. Hogg[1]

AFFILIATIONS

[1]School of Engineering, University of Glasgow, Glasgow G12 8LT, United Kingdom
[2]Department of Electronic and Electrical Engineering, University of Sheffield, 3 Solly Street, Sheffield S3 7HQ, United Kingdom
[3]Vector Photonics. Ltd, Glasgow G2 4LH, United Kingdom

[a)]Author to whom correspondence should be addressed: daehyun.kim@glasgow.ac.uk

ABSTRACT

We investigated the stable polarization-pinning properties of substrate emission InGaAs-based 980 nm multi-mode vertical-cavity surface-emitting lasers (VCSELs). For the multi-mode 40 um diameter aperture VCSELs, we introduced 30 μm wide, 9 μm depth deep trenches that are 15 μm away from the cavity aperture. The VCSELs with trench structure produced higher transverse-electric (TE) polarized light output power, as compared with transverse-magnetic (TM) polarized light output power, namely, the effective TM polarization suppression was realized. These trench-etched VCSELs exhibited a 7.5 dB orthogonal polarization suppression ratio with 16.8 mW of light output power at 60 mA of current injection. The dominant TE polarization distribution was observed in polarization-resolved near-field images of spontaneous and stimulated emission due to the induced strain by the etched trenches.

Vertical-cavity surface-emitting lasers (VCSELs) are one of the promising devices for some modern applications in 3D sensing, light detection and ranging (LiDAR), optical communication systems, and optical data storage due to a range of advantages, including a circular beam shape, single longitudinal mode operation, low manufacturing cost, and two-dimensional array operation.[1] Additionally, VCSELs have attracted great attention in photonic integrated circuit (PIC) based network-on-chip applications because of the high degree of flexibility of the integration process.[2,3] In order to employ VCSELs in polarization sensitive applications, such as the hybrid and heterogeneous photonic integration, polarized emission is required due to polarization sensitivity of integrated optics. In particular, for PICs, grating couplers and waveguide elements have polarization sensitivity leading to the requirement for polarized light sources.[4] The development of erbium doped waveguide amplifiers (EDWAs) brings further requirements for wavelength of operation (980 ± 10 nm) and >10 s mW of power.[5,6] For EDWA containing PICs, the optical coupler is a key source of power loss due to polarization selectivity.

Generally, for a VCSEL with no asymmetry, the lasing polarization states are randomly oriented in the plane of the active region.[7] Spatial-/spectral-hole-burning leads to a variation in instantaneous lasing direction, and in the case of a perfect symmetry VCSEL, equal power would be emitted in all polarization angles. With the introduction of suitable asymmetry (e.g., gain, loss, strain induced birefringence), a particular polarization is preferred temporally, leading to the light emission appearing to be linearly polarized. This may be deliberate, or unintentionally due to the consequence of variations of epitaxy, shape anisotropies, device manufacturing related strain anisotropies, or intentional strain.[8]

Polarization-pinning phenomena of VCSELs have been widely investigated experimentally and theoretically. Liao *et al.*[9] demonstrated the effect of monolithically integrated surface gratings on the performance of 850 nm multi-mode VCSELs and found that the relative optical intensity difference of the TE and TM polarization modes decreased when the period of gratings increased. Ostermann *et al.*[10] experimentally and theoretically investigated the optimum surface grating depth for TM polarization suppression of 850 nm VCSELs with the monolithically integrated surface gratings on the top of the devices (25 p-DBRs, 34 n-DBRs). The depth of the surface grating was optimized with $\lambda/4$ extra cap-layer thickness. The multi-mode VCSELs demonstrated an OPSR of 17.1 dB, an average threshold of 0.28 mA, the differential

quantum efficiency of 40%, and the maximum output power of 4.5 mW. The surface grating method has advantages of monolithic integration allowing compact optical systems.

For future hybrid integration of VCSELs into PICs, the use of a top-emitting VCSEL utilizing surface gratings poses a number of practical problems with regard to driving the VCSEL. Either a deep via through the GaAs substrate to the p-contact needs to be engineered, or electrical tracks are required upon the PIC to access the p-contact. The later introduces additional complexity to the PIC and results in local heating of the PIC (close to the diode junction, or at the interconnect tracks. If the VCSEL is to be directly modulated, increasing the RC time constant is undesirable. Additionally, only passive alignment is possible.

On the other hand, a substrate emitting VCSEL[11,12] offers significant advantages in the need for only shallow vias (9 μm c.f. 100 μm) to provide electrical access to the substrate due to the differences in thicknesses of the material. Substrate emission allows access to contacts that can be driven allowing active multi-emitter alignment. However, sub-wavelength surface gratings are not ideal for realizing polarization pinning gratings. For an epi-surface sub-wavelength grating, the ratio of the threshold gain parallel and orthogonal to the grooves (around 0.9–0.8) is critical.[10] If a substrate emission version is created either a low efficiency, high threshold design would be possible (25 p-DBR "high reflector"<25 n-DBR output coupler) or deeply etched sub-wavelength gratings are required (around 10 DBR periods). This is significantly different process than current technologies and would be expected to introduce additional scattering loss. An additional solution would be to place the grating within the cavity, e.g., at the n-DBR cavity/substrate interface. However, this is inaccessible after epitaxial growth and so would require advanced epitaxial re-growth processes posing possible yield and reliability issues. Only the former, low efficiency substrate emission devices have been realized.[13]

As a simple and low-cost process, the deep trench process can be an effective solution for polarization-pinning. Sargent *et al.*[14] observed polarization stability of 780 nm VCSELs with 13 μm aperture diameters. After trench etching and an annealing process, a uniaxially applied strain along the ⟨110⟩ crystallographic orientation affected the longitudinal Fabry–Pérot mode, the transverse photon modes, and material gain. This was evidenced by PL and Raman spectroscopy. The strain changed the overlap of the Fabry–Pérot mode and material gain in the minimum polarization orientation, resulting in a dominant polarization. Dowd *et al.*[15] investigated the polarization dependency of 850 nm VCSELs with 20 μm cavity diameters and reported the current-polarized light output power characteristics before and after trench-etching, showing no degradation in total light output power and an OPSR of ∼17 dB. Furthermore, this approach does not require sophisticated surface grating manufacture, incorporating additional lithography and etch processes, leading to higher manufacturing costs.

In this study, trench structures were employed in multi-mode substrate emitting VCSELs operating at 980 nm. Here, deeply etched trenches to allow electrical contact to the substrate also act to pin the polarization of the VCSEL. Figure 1(a) shows the final device structure with a schematic of 40 μm diameter InGaAs based substrate emission VCSEL. The trenches are 30 μm wide, 9 μm depth, and 15 μm away from the cavity aperture. The trenches allow the preferential selection of polarization by inducing stress in the devices. In this paper, trenches are aligned to the $[01\bar{1}]$ crystal axis, defining the polarization directions. Such that TE (TM) polarization is parallel (perpendicular) to the

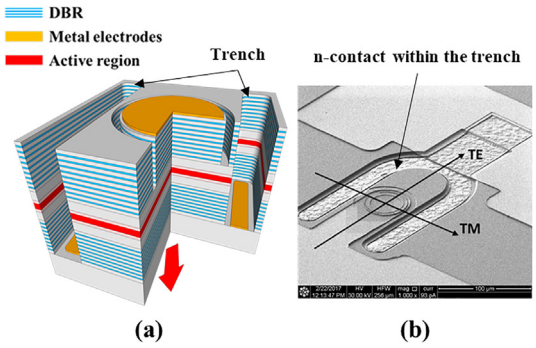

FIG. 1. Fabricated InGaAs-based VCSELs: (a) schematic diagram and (b) SEM image of the final device.

trenches, as shown in Fig. 1(b). The characteristics of the polarization-pinning were determined through current-polarized light output power measurements, polarized emission spectra, and polarized near-field imaging at below (spontaneous emission) and above threshold (lasing) current.

A metalorganic chemical vapor deposition (MOCVD) system was used to grow 980 nm InGaAs-based NIR VCSELs on the 630 μm thick n-GaAs substrate. The epilayer stack consisted of 28 pairs Si-doped n-AlGaAs ($n_d = 2 \times 10^{18}\,cm^{-3}$) distributed Bragg reflector (DBR) layers, an active region of three pairs $Ga_{0.83}In_{0.17}As/Ga_{0.08}As_{0.92}P$ multi-quantum wells, separated by 127 nm $Al_{0.3}Ga_{0.7}As$ barrier, a 70-nm-thick $Al_{0.98}Ga_{0.02}As$ oxidation layer, and 30 pairs C-doped p-AlGaAs ($n_a = 2.5 \times 10^{18}\,cm^{-3}$) DBR layers, where Al contents of the n- and p-AlGaAs layers were controlled to serve as DBRs. The DBR layers were composed of alternating high- and low-refractive index layers of $Al_{0.12}Ga_{0.88}As/Al_{0.9}Ga_{0.1}As$ multilayer. Devices were fabricated using standard contact photo-lithography. Shallow mesa structures were etched above the active region, and deep trenches were etched down to the substrate using an inductively coupled plasma reactive-ion etch (ICP-RIE) process with SiO_2 hard mask. Then, 600 nm Si_3N_4 was deposited as an insulating layer by a plasma enhanced chemical vapor deposition (PECVD). Ti/Pt/Au (20/20/200 nm) and Ni/Au/Ge/Ni/Au (5/20/130/30/150 nm) Ohmic contacts were deposited on the p-GaAs and n-GaAs layers, respectively, followed by annealing at 450 °C for 30 s. The n-contacts were deposited within trenches. Ti/Pt/Au (20/20/200 nm) bond-pads were deposited on both electrodes for wire bonding. To distinguish the orthogonally polarized TE and TM emission modes, a linear polarizer with extinction ratio of 2000 was used during the measurements.

Figure 2 shows the light output power and OPSR as a function of injection current for the trench-etched VCSELs with TE (parallel to the trench) and TM (perpendicular) polarization modes. The devices were tested at room temperature under CW operation. The threshold current values of the TE and TM polarized emission are 7.5 and 9 mA, respectively, and the polarization angle of maximum power over all currents is parallel to the trench (TE). The total light output has maximum power of 16.8 mW at 60 mA with 0.42 W/A of slope efficiency and shows thermal rollover at higher currents, which is attributed to non-ideal heatsinking and thermally induced detuning of the cavity resonance and gain peak.

The OPSR, which is calculated as the ratio of the light output power in the two polarization modes, is also plotted,

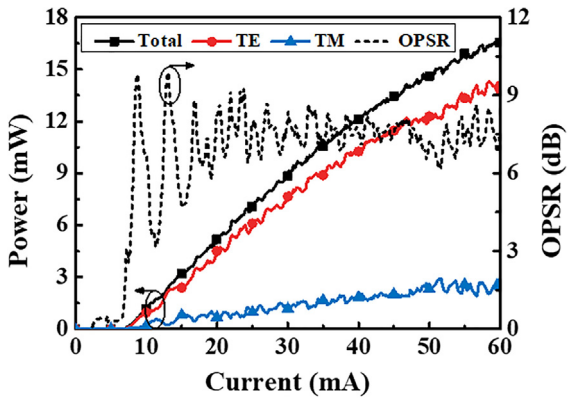

FIG. 2. The light output power- and OPSR-current characteristics of the trench-etched VCSELs with different types of polarizations.

$$\mathrm{OPSR} = 10 \log \frac{P_{TE}}{P_{TM}}. \quad (1)$$

The polarization dependent optical loss of the cavity is expected to be minimal due to the large distance (15 μm) of the trench sidewall from the optical cavity. These trench-etched VCSELs show a robust polarization ratio with an OPSR of ~7.5 dB even at high current region. The OPSR is observed to vary by ± 1 over the range of currents. This contrasts with the operation of a standard VCSEL where the OPSR sharply decreases to a low value.[15]

Polarized near-field imaging of the active region was performed below threshold current (at 4 mA) to investigate the polarization of the spontaneous emission. Figure 3 plots the relative intensity difference of the two polarization modes and is defined as

$$\Delta I = 100 \times (I_{TE} - I_{TM})/(\max I_{TM}). \quad (2)$$

It is noted that TE polarized emission is dominant across the whole of the cavity, as compared with TM polarized emission. This difference is due to the induced strain splitting the spontaneous emission (and gain) spectrum, leading to different overlap with the cavity mode and, hence, spontaneous emission intensity. This observation is in agreement with the observed difference in threshold current for the device in terms of TE and TM emission.

Figure 4 shows the TE and TM polarized emission spectra of the trench-etched VCSELs under 10, 20, and 30 mA current injection at room temperature. The number of observed modes increases as the current injection increases because of the large aperture size and multi-modal nature of the trench-etched VCSELs. It is also worth noting that the samples exhibit a redshift of the emission wavelength by ~0.7 nm as the current injection increases by 10 mA steps. That is attributed to the self-heating effect of the active region with increased current injection. From the ~1.4 nm peak shift of the emission spectra at 30 mA current injection, a junction temperature variation of 14 °C can be estimated.[16] This variation is a suitable value as a pump source for EDWA considering the absorption bandwidth of the Er^{3+} ions. The observation of an essentially constant OPSR indicates that thermally induced changes to the detuning of cavity resonance and gain peak are not limiting factors for this device. The observed splitting in the peak wavelengths for TE and TM spectra (40 ± 5 GHz) is consistent with strain being the origin of the observed polarization pinning. Splitting of up to 12 GHz has been attributed to residual anisotropic strain in nominally isotropic devices.[17] A splitting of around 40 GHz corresponds to a strain of 2.5×10^{-4}.[18]

To further investigate the lasing characteristics of the device, polarized near-field imaging was carried out above threshold current. Figure 5 plots the near-field images of the TE and TM polarization

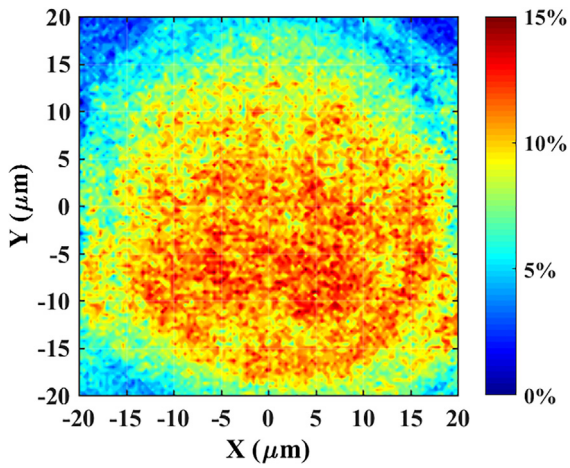

FIG. 3. Relative intensity difference of TE and TM polarization modes for spontaneous emission.

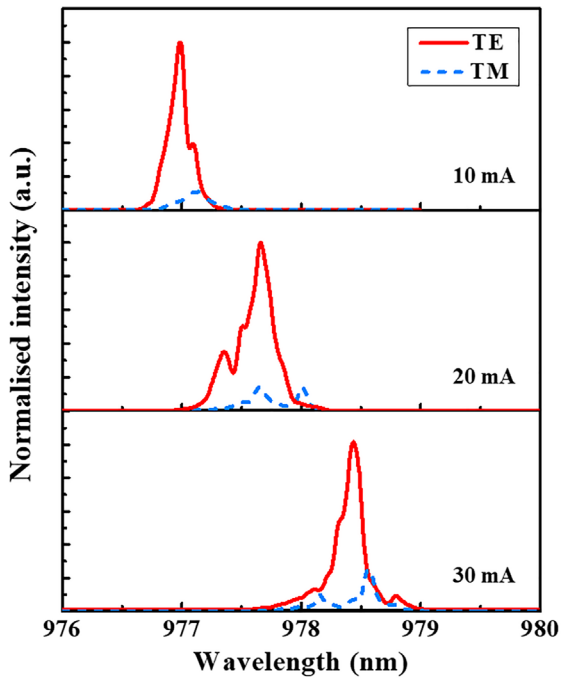

FIG. 4. The EL spectra of the TE and TM polarization at 10, 20, and 30 mA current injection.

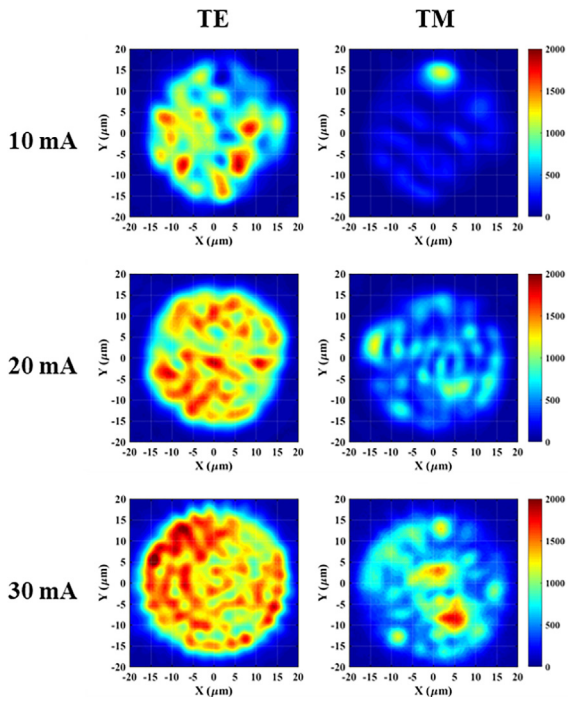

FIG. 5. The near-field images of the TE and TM mode emission at 10, 20, and 30 mA current injection.

modes at 10, 20, and 30 mA current injection with RGB color-coded intensity contour mapping. Generally, at a given current, there is a spatial correspondence with polarization intensity, i.e., there is an anti-correlation between high TE and TM lasing emission regions. Additionally, at any given current, the TM image has fewer lasing modes, and this is also evidenced in the emission spectra. As current is increased (with the 10 mA steps shown here), it is observed that modes associated with a given polarization are not fixed in place, and there is a variation in mode pattern. For much smaller current steps, the polarized spatial images and polarized emission spectra can be correlated, and this is the subject of further study.

It is expected that polarized multi-mode emission is a complex interaction of current spreading, spatial-/spectral-hole-burning, and the influence of strong thermal gradients in the cavity as the current injection is increased.[19–21] The lack of correlation between polarized spontaneous emission (Fig. 3) and stimulated emission mapping is a testament to this as the movement of polarization "hotspots" and the observed variation in OPSR in Fig. 2.

The results of the EL spectra and near-field images show robust TE polarization-pinning of the trench-etched substrate emission VCSELs. This can be ascribed to the strain induced splitting of modal gain spectra, and this is effectively achieved over essentially the whole of the 40-um diameter of the junction through the introduction of the deep trenches (that also serve to provide electrical access to the n-GaAs substrate). The etched trenches allow the relaxation of tensile strain introduced during the growth process in the $[01\bar{1}]$ direction of the standard (001) GaAs wafer.[14] The induced stress in the active region leads to the shift of the band edges. These combined effects result in effective polarization-pinning with separate gain spectra and different transverse mode distribution of the TE and TM polarization modes. These preliminary results indicate modest (<10 dB) OPSR, as compared to >20 dB achievable for sub-wavelength surface gratings. Future work to enhance this value will involve the exploration of even greater etch depths, bringing the etched trench closer to the active element, and use of strained isolation dielectrics.

The polarization-pinning properties of the substrate emission InGaAs-based 980 nm multi-mode VCSELs have been reported. These trench-etched VCSELs provided effective TM polarization suppression due to a strain induced gain spectrum shift. The preferential selection of polarization was highlighted with separate longitudinal and transverse modes of the TE and TM polarization modes. At the 60 mA of current injection, a 7.5 dB OPSR with 16.8 mW of light output power was achieved. The introduction of the deep trenches around substrate emitting VCSEL apertures is a suitable method for polarization sensitive applications where substrate emission is required.

This work was supported through the Engineering and Physical Sciences Research Council (EPSRC) of U.K. (No. EP/M015165/1).

AUTHOR DECLARATIONS

Conflict of Interest

The authors have no conflicts to disclose.

DATA AVAILABILITY

The data that support the findings of this study are available within the article.

REFERENCES

[1]J. L. Jewell, J. P. Harbison, A. Scherer, Y. H. Lee, and L. T. Florez, IEEE J. Quantum Electron. **27**, 1332 (1991).
[2]H. Lu, J. S. Lee, Y. Zhao, C. Scarcella, P. Cardile, A. Daly, M. Ortsiefer, L. Carroll, and P. O'Brien, Opt. Express **24**, 16258 (2016).
[3]M. R. Billah, M. Blaicher, T. Hoose, P.-I. Dietrich, P. Marin-Palomo, N. Lindenmann, A. Nesic, A. Hofmann, U. Troppenz, M. Moehrle, S. Randel, W. Freude, and C. Koos, Optica **5**, 876 (2018).
[4]Q. Wei, J. Xiao, D. Yang, and K. Cai, Opt. Eng. **60**, 067104 (2021).
[5]A. Polman, J. Appl. Phys. **82**, 1 (1997).
[6]S. A. Kamil, J. Chandrappan, M. Murray, P. Steenson, T. F. Krauss, and G. Jose, Opt. Lett. **41**, 4684 (2016).
[7]C. J. Chang-Hasnain, J. P. Harbison, L. T. Florez, and N. G. Stoffel, Electron. Lett. **27**, 163 (1991).
[8]K. D. Choquette, R. P. Schneider, L. L. Kevin, and R. E. Leibenguth, IEEE J. Sel. Top. Quantum Electron. **1**, 661 (1995).
[9]W. Liao, C. Li, J. Li, X. Guo, W. Guo, X. Wei, and M. Tan, Appl. Phys. B **127**, 23 (2021).
[10]J. M. Ostermann, P. Debernardi, and R. Michalzik, IEEE J. Quantum Electron. **42**, 690 (2006).
[11]M. Grabherr, M. Miller, R. Jäger, R. Michalzik, U. Martin, H. J. Unold, and K. J. Ebeling, IEEE J. Sel. Top. Quantum Electron. **5**, 495 (1999).
[12]M. Grabherr, R. Jäger, M. Miller, C. Thalmaier, J. Heerlein, R. Michalzik, and K. J. Ebeling, IEEE Photonics Technol. Lett. **10**, 1061 (1998).
[13]T. Mukaihara, N. Ohnoki, Y. Hayashi, N. Hatori, F. Koyama, and K. Iga, IEEE J. Sel. Top. Quantum Electron. **1**, 667 (1995).
[14]L. J. Sargent, J. M. Rorison, M. Kuball, R. V. Penty, I. H. White, S. W. W. Corzine, M. R. T. Tan, S. Y. Wang, and P. J. Heard, Appl. Phys. Lett. **76**, 400 (2000).

[15]P. Dowd, P. J. Heard, J. A. Nicholson, L. Raddatz, I. H. White, R. V. Penty, J. C. C. Day, G. C. Allen, S. W. Corzine, and M. R. T. Tan, Electron. Lett. **33**, 1315 (1997).
[16]T. Sale, *Vertical Cavity Surface Emitting Lasers* (Wiley, New York, 1995).
[17]A. K. J. Van Doorn, M. P. Van Exter, and J. P. Woerdman, Appl. Phys. Lett. **69**, 1041 (1996).
[18]M. Peeters, K. P. Panajotov, G. Verschaffelt, B. Nagler, J. Albert, H. Thienpont, I. P. Veretennicoff, and J. Danckaert, Proc. SPIE **4649**, 281 (2002).
[19]C. Degen, B. Krauskopf, G. Jennemann, I. Fischer, and W. Elsäßer, J. Opt. B **2**, 517 (2000).
[20]C. Degen, I. Fischer, and W. Elsäßer, Appl. Phys. Lett. **76**, 3352 (2000).
[21]C. Degen, W. Elsaber, and I. Fischer, Opt. Express **5**, 38 (1999).